Detection of Depth of the Tumor in Microwave Imaging Using Ground Penetrating Radar Algorithm

Vanaja Selvaraj[1, *], Joselin J. Sheela[2], Rahul Krishnan[1],
Lalitha Kandasamy[3], and Sasirekha Devarajulu[4]

Abstract—Microwave Imaging (MI) is a new technique for detecting breast cancer using electrical property difference between the non-malignant and malignant tissues present in the breast. Numerous studies show that detecting the depth of the tumor is the essential measure in determining additional management. Developing evidence in many of the literature surveys illustrate that detecting tumor depth is a precise parameter for identifying the affected area. Thus, Ground Penetrating Radar (GPR) algorithm is applied successfully to detect the exact depth of the malignant tissue. Generally, GPR is originally conceived for archaeological investigations, building condition assessment, detection of buried mines, etc. But here an effort has been made to apply GPR to Radar-based breast cancer detection. The simulated bandwidth of the proposed UWB antenna starts at 2.4 GHz and ends at 4.7 GHz. The electromagnetic wave reflected due to dielectric property variation is used by GPR algorithm to identify the depth of the tumor. Before applying a depth migration technique, preprocessing steps like Cartesian form transformation, Hermitian Signal Processing, and Inverse Fast Fourier Transform (IFFT) have to be followed in the backscattered signal to convert positive frequency data into time-domain data. Depth details can be noticed in the migrated image, after applying the migration procedure. Results show that GPR algorithm can be effectively used for detecting the tumor embedded in the depth of the breast tissue. To understand the effectiveness of this imaging scheme, an experimental analysis is done using a combination of wheat flour and water-petroleum jelly. The measured impedance bandwidth of the UWB antenna ranges from 2.8 GHz to 4.48 GHz. The observation is done for a known spherical tumor of diameter 13 mm which is placed at different depths from the skin layer. While applying the algorithm in the received backscattered signal, we were able to detect correctly the tumor at a depth of 45 mm embedded in the breast tissue. The experimental results are compared with simulation ones to validate the aptness of a microwave imaging approach for detecting the depth of the tumor.

1. INTRODUCTION

In the worldwide range, the second leading source of dangerous cancer disease among women is breast cancer. There are several ways to detect breast cancer. But still, X-ray mammography is the maximum frequently used diagnostic method for breast cancer. However, mammography is a somewhat painful method involving high-intensity ionizing radiation and therefore may cause cancer to the healthy tissues [1–4]. To overcome these difficulties, radar-based microwave imaging technique has been developed. Radar technique is used to detect land mines, groundwater, presence of injuries, respiratory motion from a remote place, imaging the human body, etc. [5, 6]. Here, the radar method

[1] Department of Electronics and Communication Engineering, Rajalakshmi Institute of Technology, Chennai-600124, India.
[2] Department of Electronics and Communication Engineering, R.M.K. Engineering College, Chennai, India. [3] Department of Electronics and Communication Engineering, SRM Institute of Science and Technology, Chennai, India. [4] Department of Electronics and Communication Engineering, Rajalakshmi Engineering College, Chennai, India.

is used to image the breast tissue. The radar approach involves transmitting the short duration pulse from the antenna into the breast tissue. The signal processing method is followed to the received backscattered signal to detect the highly scattering region i.e., malignant tumor.

Various imaging techniques and algorithms are there to identify the depth of the tumor. Microwave Imaging via Space-Time (MIST) beamforming algorithm [7], Parallel plate waveguide port technique [8], Time of Arrival (TOA) data fusion method [9, 10], Delay and Sum (DAS) beamforming algorithm [11], etc. can be used to detect the depth of the tumor. On the other hand, the above techniques have numerous restrictions. Complex antenna array arrangement is required for tumor detection, and designing an ultra-wideband (UWB) antenna is challenging. Moreover, the array setup is highly exorbitant and requires more time to detect the tumor.

The present article pivoted mainly through a single antenna to localize the tumor by easily applying GPR algorithm. The image obtained using the GPR algorithm is called B-scan. Design and simulation of the UWB antenna and breast phantom are evolved with Computer Simulation Technology (CST) software [12]. MATLAB simulation software is used to reconstruct the image from the Backscattered signal.

2. METHODOLOGY

The Radar technique can be successfully used to locate the target from the backscattered microwaves [13]. Figure 1 shows the basic principle behind the microwave imaging which is scattering microwaves when a wave enters from the region of excessive dielectric constant to the region of less dielectric constant.

Scattered microwaves are received by the same antenna, which acts as a transmitter, and it is processed to create an image which distinguishes the location of the strong reflections (tumor) from normal tissue. Figure 2 shows the steps involved in microwave imaging, and the following contents will explain in brief about each component involved in microwave breast imaging.
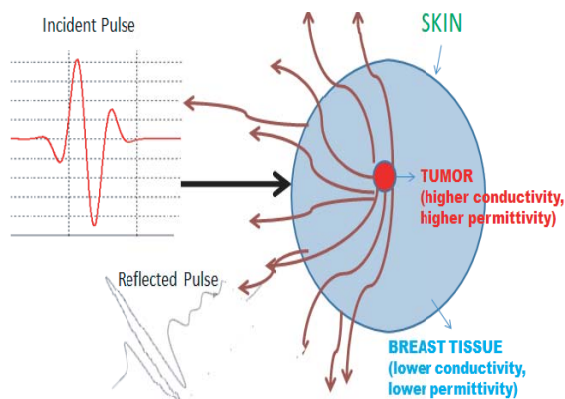

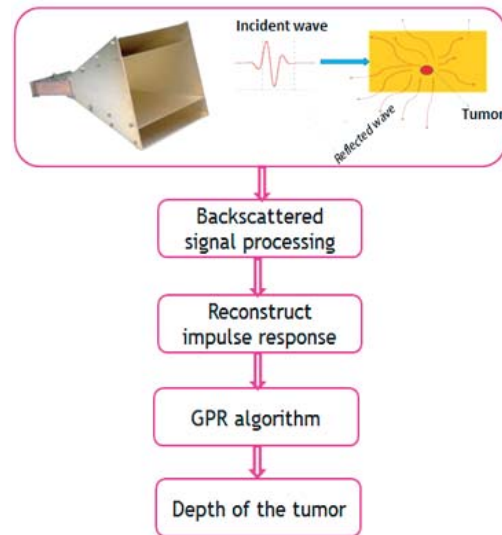**Figure 1.** Principle of microwave imaging.

Figure 2. Flow diagram of microwave breast imaging.

2.1. Ultra Wideband Antenna

The microwave imaging technique uses UWB antenna [14, 15] which covers a band of frequencies from 2.4 to 4.7 GHz as shown in Figure 3. The low frequency range is required to make sure of deep penetration [16] which is favourable for identifying the tumors at deep location, whereas high-frequency
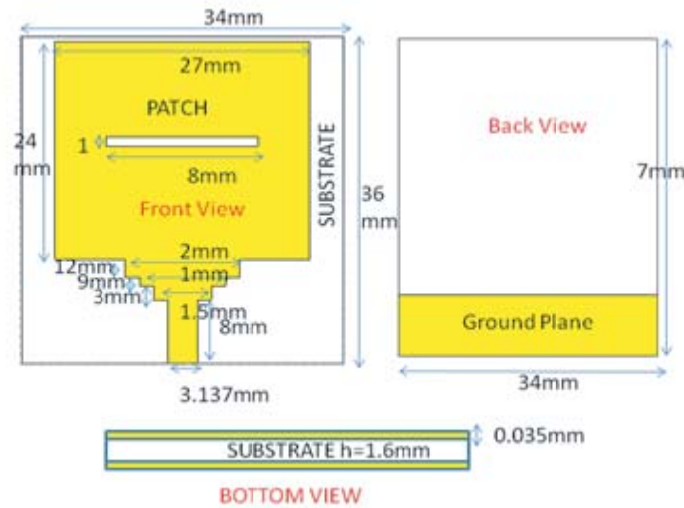
Figure 3. Designed antenna and its dimension.

band is essential in order to obtain acceptable spatial resolution which is also favourable for identifying tumors neighbouring to the skin level.

2.2. Breast Tissue

The anatomy of the breast has been analyzed in order to design breast phantom for imaging. Homogenous phantom which mimics the dielectric constant of the breast phantom is designed [17], and it accounts for only adipose tissue, so as to avoid the system complexity. Figure 4 shows the locations of the antenna and tumor to be placed in the breast tissue.
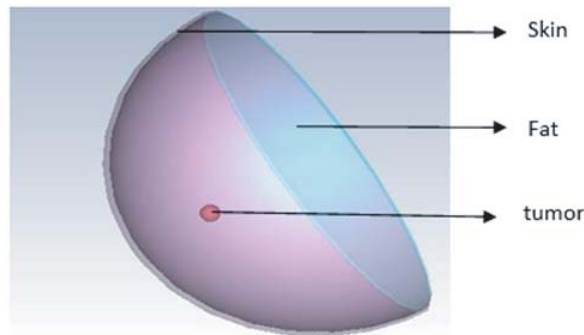

Figure 4. Structure of homogeneous breast tissue.

All measurements are taken with a numerical homogenous hemispherical breast phantom. Initially, a skin layer of thickness 1 mm is designed with a radius 60 mm. Then the space inside the skin layer is filled by fat. A spherical shape tumor of radius 3 mm is placed in the fat layer. The tumor is set in the breast phantom at a depth of 25 mm which is designed in CST Microwave studio 2010.

The Debye first-order differential Equation (1) is embraced with the dielectric properties of the frequency dependence materials.

$$\varepsilon_r - j\frac{\sigma}{\omega\varepsilon_0} = \varepsilon_\infty + \frac{\varepsilon_s - \varepsilon_\infty}{1 + j\omega\tau} \tag{1}$$

The dielectric constants of the skin, fat, and malignant tissue are calculated at a center frequency of 3.55 GHz.

For skin: Relative permittivity $(\varepsilon_r) = 36.963$ and conductivity $(\sigma) = 2.0551\,\text{S/m}$;
For fat: Relative permittivity $(\varepsilon_r) = 4.9289$ and conductivity $(\sigma) = 0.22391\,\text{S/m}$;
For tumor: Relative permittivity $(\varepsilon_r) = 51.382$ and conductivity $(\sigma) = 2.6615\,\text{S/m}$.

2.3. Physical Model of Breast Phantom

The microwave signal produced from the UWB antenna interacts with the breast phantom. For the analysis of the depth of the tumor, a hemispherical breast phantom is placed above the UWB antenna as shown in Figure 5.
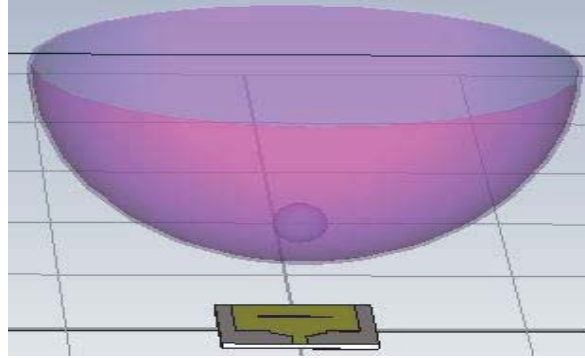
Figure 5. Hemispherical breast phantom with a transmitter.

2.4. Backscattered Signal Processing

The various steps involved in the reflected signal preprocessing stage are shown in Figure 6. The reflected signal obtained after the simulation is in the frequency domain. For radar-based signal processing, the information has to be in the time domain. As S_{11} has positive frequency data, a preprocessing step has to be implemented for Inverse Fast Fourier Transform (IFFT) and attain the impulse response of the reflected data. The preprocessing phases are followed in advance of applying the IFFT technique, shown in Figure 6.
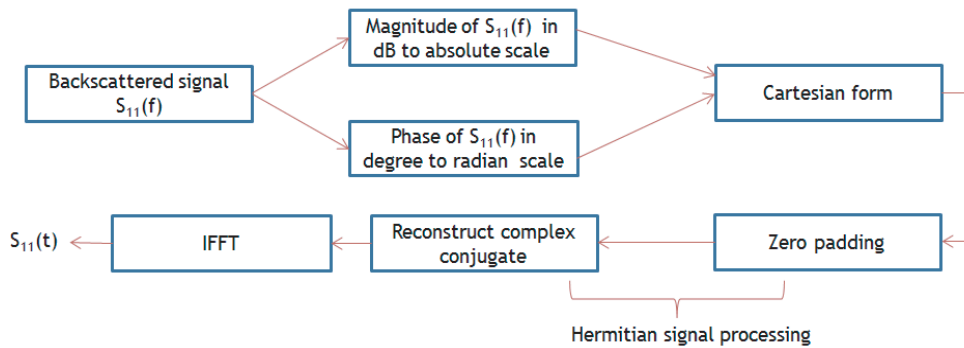
Figure 6. Steps for signal pre-processing.

2.5. Conversion of S_{11} Parameter

The reflected wave acquired using an antenna is in polar configuration $(|(f)|$ phase $(f))$. Therefore, the magnitude of the reflected signal (S_{11}) in the dB scale is transformed to an absolute scale. The reflected signal's phase constraints which are in the form of degree scale are transformed into radian scale. Hence, for further processing steps, S_{11} is converted into Cartesian nature $z = a + bj$.

3. HERMITIAN SIGNAL PROCESSING PROCEDURE

According to the Hermitian technique, the Fourier Transform (FT) function of the real value function is symmetric in nature. As the impulse response $S_{11}(t)$ is a real-valued function, the frequency (f) has to be Hermitian symmetric. Though the entire frequency (f) ranges from $[-f_{stop}, f_{stop}]$, the information acquired from the $S_{11}(f)$ has merely the positive frequency ranges. The negative value frequency ranges are dispensable of the positive value frequencies. So to achieve the impulse function $S_{11}(t)$, frequency values ranges from $[-f_{stop}, f_{stop}]$ must be formed, shown in the following Figure 7. $S_{11}(f)$ frequency differs in the range from f_{start} to f_{stop} which is shown in Figure 7(a). To begin with, zero padding process to be done in between the frequency of $[0, f_{start}]$ which is shown in Figure 7(b). The number of zeros to be added for the zero padding process is considered in the subsequent equation:

$$\text{Number of zeros to be padded} = \frac{f_{start}}{\Delta f - 1} \tag{2}$$

where Δf is the step frequency which can be defined as $\Delta f = f(2) - f(1)$.

Once zero padding process is completed, $S_{11}(f)$ is acquired for the range of frequencies from $f = [0, f_{stop}]$. The following steps are followed to create $S_{11}(f)$ for the frequency range from $f = [-f_{stop}, 0]$. It is attained by following Hermitian signal property, and the obtained $S_{11}(f)$ is displayed in Figure 7(c). Time-domain impulse function which can be acquired by means of the function IFFT is displayed in Figure 7(d).
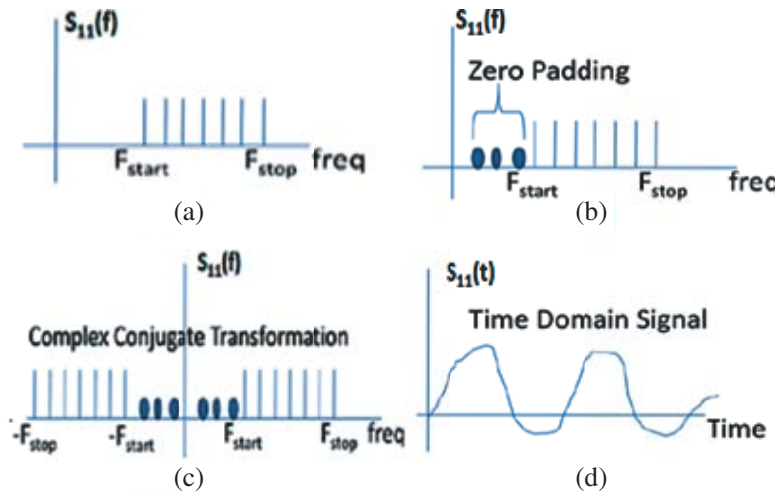

Figure 7. Backscattered signal pre-processing steps, (a) acquired S_{11} signal, (b) zero padded signal, (c) complex conjugate signal and (d) $S_{11}(t)$ signal.

4. RECONSTRUCT IMPULSE RESPONSE

The backscattered signal can be easily transformed from the frequency-domain into the time-domain using the process of inverse Fourier Transform. The goal of this work is to process the backscattered signal and finally conclude the exact location of the target present inside the breast phantom. The various steps involved to reform the impulse response of the reflected signal are shown in Figure 8.

For the determination of the depth of the tumor, two different types of the reflected signals are taken from the breast phantom. One of the reflected signal readings is taken from the breast without a tumor, and the other one is taken with the tumor. Then the Hermitian signal processing scheme and IFFT are applied in both the backscattered signals. Eventually, the impulse response of the backscattered signal is the combination of different responses like a transmitted signal, noise disturbance, antenna cross-coupling factors, and the reaction of tumor response. The tumor response factor is very small compared to the other background response. In order to enhance the tumor response, subtract the
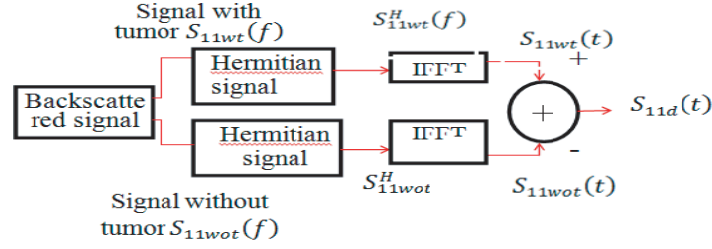
Figure 8. Reconstruction of impulse response.

impulse response of the backscattered signal with and without tumor, i.e., the impulse response due to the tumor is obtained in this way.

$$S_{11d}(t) = S_{11wt}(t) - S_{11wot}(t) \tag{3}$$

where $S_{11wt}(t)$ is the impulse response of the backscattered signal with tumor, and $S_{11wot}(t)$ denotes the impulse response factor of the backscattered signal without tumor.

4.1. Estimation of GPR Depth Algorithm

GPR algorithm is used to estimate the depth of the tumor. The migration imaging procedure followed to obtain the real location of the target is the Frequency-Wavenumber image migration (F-K) technique. In this migration technique, horizontal location is represented against the windowed backscattered signal to acquire the depth of the tumor. In this case, the minimum target depth and the maximum are put down as $[z_{min}, z_{max}]$ shown in Figure 9.
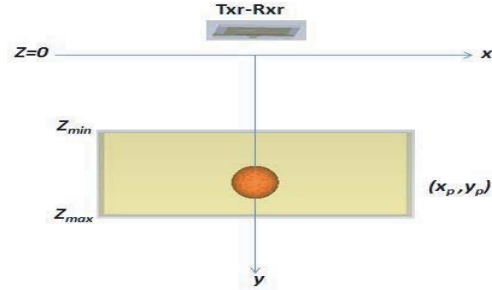

Figure 9. Environmental medium for imaging.

Time resolution (Δt) and depth resolution (Δd) of the discrete impulse response of the resultant backscattered signal $S_{11d}(t)$ are applied as

$$\Delta t = 1/f_s \tag{4}$$

where f_s is the sampling frequency.

$$f_s = 3 * f_{stop} \tag{5}$$

The depth resolution is calculated as

$$\Delta d = v * \Delta t/2 \tag{6}$$

where v is the electromagnetic wave velocity.

By means of the depth resolution (Δd), an expected depth vector $z = (0 : 4087) * \Delta d$ can be calculated. Eventually, using the following equation, the collected data are windowed as

$$\text{Windowed signal} = \begin{cases} \text{Backscattered } (S_{11d}(t)) & q_{min} < \text{ signal } < q_{min} \\ 0 & \text{Otherwise} \end{cases} \tag{7}$$

where, $q_{min} = \frac{z_{min}}{\Delta d}$ and $q_{max} = \frac{z_{max}}{\Delta d}$.

Afterwards, the depth of the tumor details can be obtained from the image by plotting the reflected signal with orientation to X location.

5. RESULT AND DISCUSSION

In hemispherical breast phantom, the tumor depth is detected through the simulation process. The different steps to be accompanied for the tumor depth detection are as follows.

5.1. Backscattered Signal Preprocessing

To conclude the depth of the tumor, two different types of reflected signals have to be taken from the hemispherical shape breast phantom. One of the reflected signal readings is taken from the breast phantom without a tumor, and the other one is taken from the breast phantom with a tumor. For determining the reflected signal from the breast phantom without tumor, a hemispherical shape homogeneous breast phantom is located at a space of 22 mm above the antenna. The released EM wave from the antenna is scattered, transmitted, and reflected at the superficial of the breast phantom. This reflected signal is received by the same antenna which is used for transmission. The magnitude and phase of the received signal are shown in Figure 10.
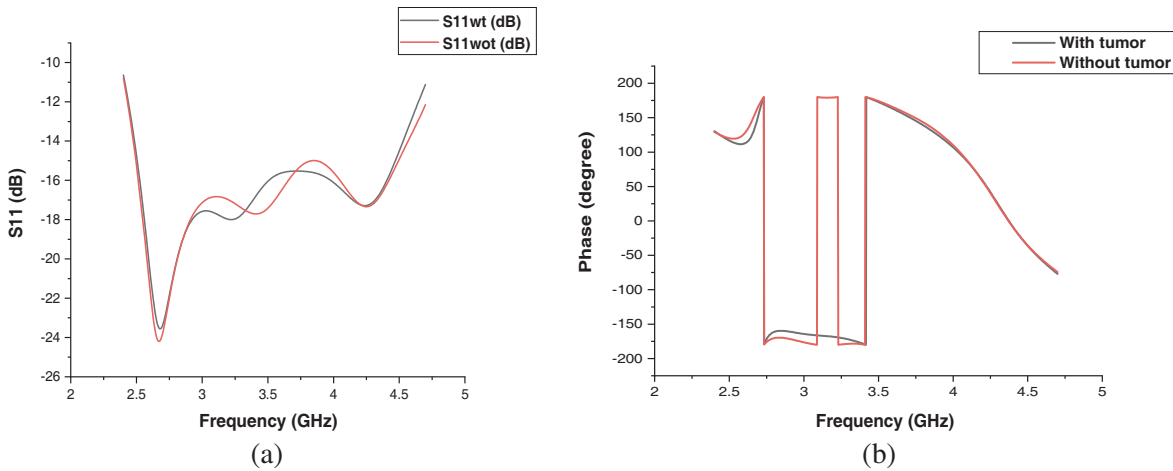

Figure 10. Backscattered signal with and without tumor (a) magnitude and (b) phase.

The quantitative results of reflected signal with and without tumor are shown in Table 1. The magnitude of the reflected signal obtained for the analysis is in a negative value. The magnitude of the reflected signal without tumor is -24.2 dB whereas with the tumor it is -23.56 dB. A high level of negative value constitutes a lesser amount of power which is reflected from the phantom while a low level represents greater amount of power which is reflected from the breast phantom. This is mainly due to more dielectric properties of the tumor tissue. Similarly, a shift in frequency of the reflected signal happens when there is an increase in dielectric property.

Table 1. Comparison of reflected signal with and without tumor for simulation.

Reflected signal	Without Tumor	With Tumor
Magnitude of S_{11} (dB)	-24.2	-23.56
Frequency (GHz)	2.667	2.692

The entire frequency range of the backscattered signal $S_{11wot}(f)$ is of positive frequency $f_{start} = 2.4$ GHz and $f_{stop} = 4.7$ GHz with the step frequency $\Delta f = 2.3$ MHz. The number of sample points generated from the signal is 1001. So to compute the impulse response $S_{11wot}(t)$, the frequency (f) has to be in between $[-f_{stop}, f_{stop}]$. Firstly, zero padding has to be done between the frequencies from $[0, f_{start}]$. The number of zeros to be padded between 0 and 2.4 GHz is 1043. Once zero padded, $S_{11wot}(f)$

will be obtained for the frequency (f) between $[0, f_{stop}]$. Therefore, the total number of samples present between $[0, f_{stop}]$ is 2044 (1043 + 1001). The following level is to produce $S_{11wot}(f)$ for the frequency (f) between $[-f_{stop}, 0]$. It is obtained besides the Hermitian property. Therefore, the complete spectrum of $S_{11wot}(f)$ is generated for the frequency (f) between $[-f_{stop}, f_{stop}]$ with the total number of samples 4088. The IFFT of the signal $S_{11wot}(t)$ can be computed, when the complete spectrum of the signal is produced.

Then a known spherical tumor of radius 10 mm is located inside the phantom which is placed at a depth of 22 mm from the skin layer. The reflected signals, magnitude, and phase information received by the antenna after the simulation are displayed in Figure 10. Then Hermitian signal processing and IFFT in the backscattered signal ($S_{11wt}(f)$) with a tumor is applied. Next, the impulse response due to the tumor alone is calculated by making the difference between the impulse responses of the backscattered signal with and without tumor. The signal of tumor in the 1D waveform for the simulation analysis is shown in Figure 11.
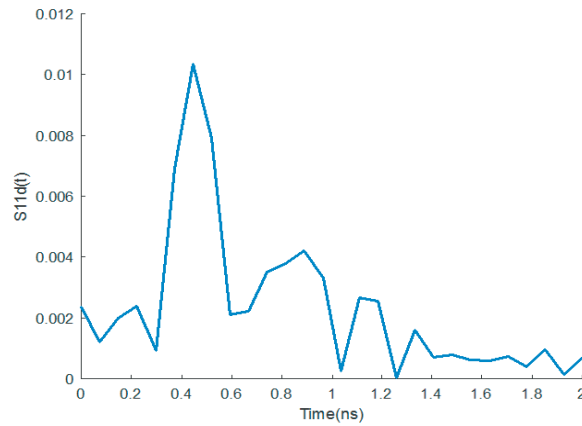

Figure 11. Impulse response of the tumor in 1D waveform.

5.2. GPR Depth Estimation

The exact depth of the tumor can be obtained by depth migration technique. The impulse response due to the tumor alone is given as an input to the image focusing procedure. Here, the minimum target depth and the maximum are considered as $[z_{min} = 24\,\text{mm}, z_{max} = 74\,\text{mm}]$ which is set. The difference in backscattered signals with and without tumor $S_{11d}(t)$ is discrete in nature. The time resolution of the difference in backscattered signal is $\Delta t = (1/(3 \times 4.7 \times 10^9)) = 0.0709\,\text{ns}$. Therefore, for the entire total number of 4088 samples, the time resolution is 290 ns (i.e., 0.0709 ns * 4088).

The depth resolution is calculated using Equation (6) as ($\Delta d = 0.0106\,\text{m}$), and expected depth vector is calculated as $z = (0 : 4087) \times 0.0106\,\text{m}$. Eventually, using Equation (7) the gathered information is windowed in the middle of the minimum depth range and maximum, with $q_{min} = 24\,\text{mm}/\Delta d$ and $q_{max} = 74\,\text{mm}/\Delta\text{d}$. Afterward, for obtaining the depth of the tumor image, the windowed resulting signal is graphed in regards to the X position which is shown in Figure 12. It is likely to see the depth of the tumor as 22 mm from the image. Similarly, the tumor in the breast phantom at a depth of $z = 33\,\text{mm}$ is analyzed. The reconstructed image obtained from the backscattered signal by following the different steps like signal pre-processing, reconstruction impulse response, and GPR algorithm is shown in Figure 12.

6. EXPERIMENTAL ANALYSIS

The following section discusses the practical measurements in identifying the tumor in the phantom. The experimental setup of the whole system to measure the reflected signal is shown in Figure 13. In the experimental analysis, for measuring S_{11} from the breast phantom, the VNA E8363B is used. During
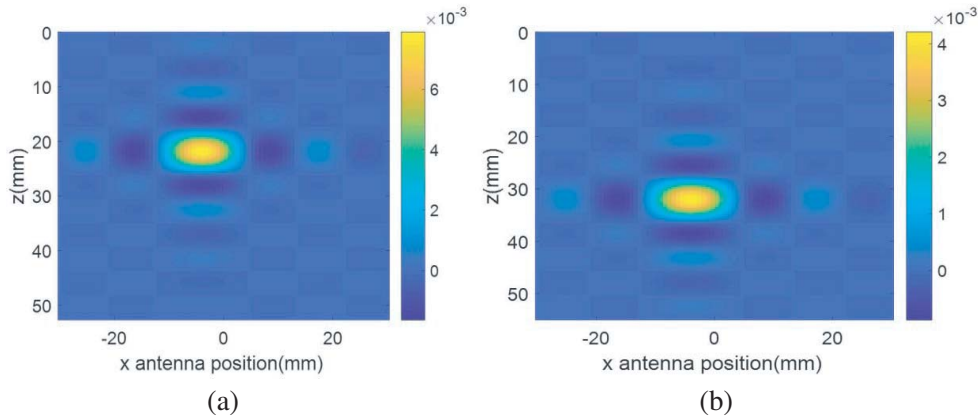
Figure 12. Reconstructed image with a tumor at the depth of 22 mm and 33 mm.

Figure 13. Experimental scenario.

measurement, the UWB antenna is placed directly above the locality of the phantom. The measured impedance bandwidth of the UWB antenna ranges from 2.8 GHz to 4.48 GHz.

To receive and transmit the EM wave, the end terminal of the VNA is connected with UWB antenna. The frequency range from 2.4 GHz to 4.7 GHz is adjusted in VNA. Initially, the antenna is placed directly above the locality of the phantom without tumor which is located at a space of 20 mm. The transmitting antenna is located at the focus of the phantom. The UWB antenna illuminates the phantom using a microwave signal. The reflected signal (S_{11}) is taken down by the same antenna which is used for transmission in the range of frequency from 2.4 GHz to 4.7 GHz. The magnitude and phase of the received signals with and without tumor are shown in Figure 14.

The quantitative results of reflected signal with and without tumor for the experiment are shown in Table 2. The magnitude of the reflected signal without tumor is -34.13 dB whereas with a tumor it is -28.92 dB. Similarly, the frequency of the reflected signal without tumor is 3.539 GHz whereas with a tumor it is 3.723 GHz. This is because conductivity (σ) and relative permittivity (ε_r) of the tumor tissue is significantly larger than a normal tissue. The larger the size of the tumor is, the greater the amount of reflected power will be.

Table 2. Comparison of reflected signal with and without tumor for experiment.

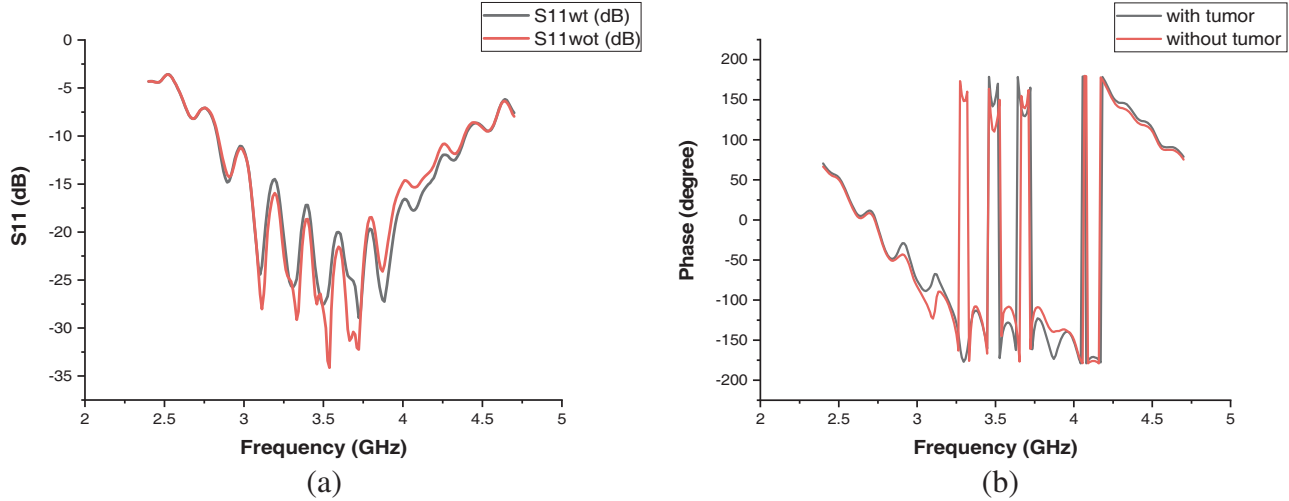| Reflected signal	Without Tumor	With Tumor
Magnitude of S_{11} (dB)	-34.13	-28.92
Frequency (GHz)	3.539	3.723

Figure 14. Measured backscattered signals with and without tumor, (a) magnitude and (b) phase.

The entire breast tissue dielectric properties increase based on the existence of the tumor tissue. When the breast tissue having tumor is exposed to microwave signal, tumor having high water content will cause significant amount of microwave scattering compared to the low water content normal tissue. Depending on the size of the tumor structure, cross sectional area for the microwave scattering process is also enlarged, thereby supporting the detection of depth of the tumor using microwave imaging. The amount of scattered information gathered from the tumor response is based on the dielectric properties of the tumor in addition to the surrounding tissue and size of the tumor.

The entire frequency range of the backscattered signal $S_{11wot}(f)$ is of positive frequency $f_{start} = 2.4$ GHz and $f_{stop} = 4.7$ GHz with the step frequency $\Delta f = 11.5$ MHz. The number of sample points generated from the signal is 201. To estimate the impulse response $S_{11wot}(t)$, (f) ranges from $[-f_{stop}, f_{stop}]$. Firstly, zero padding has to be done between the frequencies from $[0, f_{start}]$. The number of zeros to be padded between 0 and 2.4 GHz is 209. Once zero padded, $S_{11wot}(f)$ is obtained for the frequency (f) between $[0, f_{stop}]$. Therefore, the total number of samples present between $[0, f_{stop}]$ is 410. The following level is to produce $S_{11wot}(f)$ aimed at the frequency (f) between $[-f_{stop}, 0]$. It is obtained by means of Hermitian signal property. Therefore, the complete spectrum of $S_{11wot}(f)$ is generated for the frequency (f) between $[-f_{stop}, f_{stop}]$ with a total number of samples 820.

The complete spectrum of $S_{11wot}(f)$ is generated using Hermitian Signal Processing for the frequency (f) between $[-f_{stop}, f_{stop}]$. $S_{11wot}(t)$ is estimated using IFFT. For determining the backscattered signal from the phantom with the tumor, a known spherical tumor of diameter 13 mm is placed inside the phantom at a depth of 23 mm from the skin layer. The magnitude and phase of the reflected signal are shown in Figure 14. Hermitian signal processing is applied and IFFT in the backscattered signal with a tumor $(S_{11wt}(f))$. The difference between the impulse responses of the backscattered signal with and without tumor $S_{11d}(t)$ is converted into an image using an algorithm. The signal of the tumor in the 1D waveform for the experimental analysis is shown in Figure 15.

For applying image migration algorithm, minimum target depth and maximum are fixed as $[z_{min} = 20$ mm, $z_{max} = 80$ mm$]$. The difference in signal $S_{11d}(t)$ obtained is discrete in nature, and the time resolution can be $\Delta t = (1/(3 \times 4.7 \times 10^9)) = 0.0709$ ns. Therefore, for the complete 810 samples, the time resolution is 57.429 ns (i.e., 0.0709 ns $\times$ 810).

By means of the depth resolution ($\Delta d = 0.0106$ m), an expected depth vector $z = (0 : 809) \times 0.0106$ can be calculated. Eventually, using Equation (7) the gathered information is windowed in the middle of the minimum depth range and maximum, with $q_{min} = 20$ mm$/\Delta d$ and $q_{max} = 80$ mm$/\Delta d$. Afterward, the resulting processed signal is graphed in X position in order to obtain the tumor depth details from the image which is shown in Figure 16(a). It is likely to see the depth of the tumor as 18 mm from the image. Similarly, the tumor in the breast phantom is at depths of 40 mm, 45 mm, and 32 mm which is analyzed and displayed in Figures 16(b), (c), and (d).
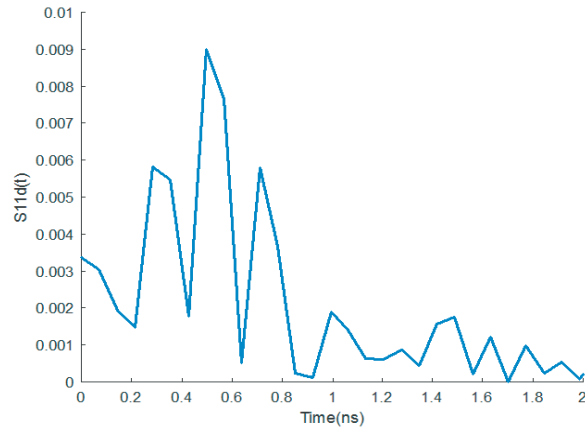
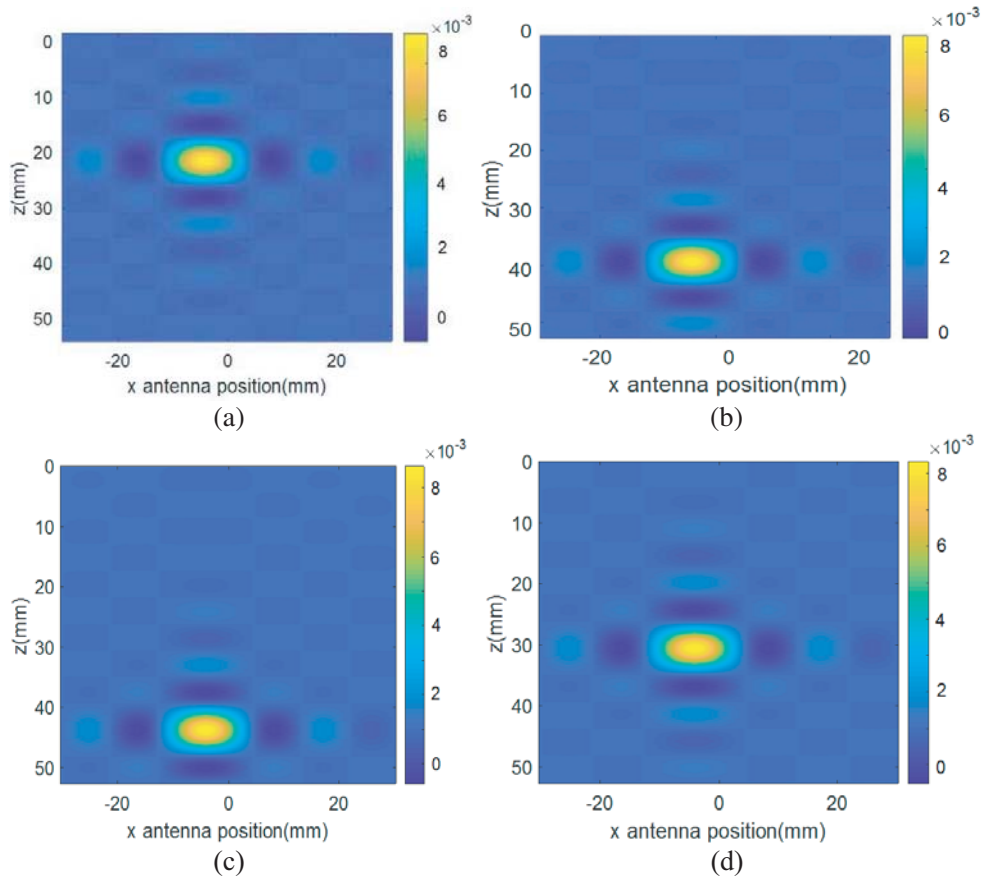**Figure 15.** Impulse response of the tumor in 1D waveform.

Figure 16. Reconstructed image with a tumor at the depth of 23 mm, 40 mm, 45 mm, and 32 mm.

7. CONCLUSION

The microwave imaging technique to detect the tumor on the basis of dielectric property variation between tumor and surrounding tissue is considered here. A UWB antenna is designed, and the $(S_{11} < -10\,\text{dB})$ bandwidth ranges from 2.4 to 4.7 GHz. A homogeneous rectangular breast model with skin, fat, and tumor tissue is created using cost beneficial material. This technique can measure reflected signal from tumor located phantom. The measured data are used to detect the depth of the

tumor. A tumor at a depth of 45 mm can be detected using this technique. Later, the same technique is followed to identify the tumor depth in the heterogeneous phantom.

REFERENCES

1. Mendat, C. C., D. Mislan, and L. Hession-Kunz, "Patient comfort from the technologist perspective: Factors to consider in mammographic imaging," *International Journal of Women's Health*, Vol. 9, 359, 2017.

2. Chan, H. H., G. Lo, and P. S. Cheung, "Is pain from mammography reduced by the use of a radiolucent MammoPad? Local experience in Hong Kong," *Hong Kong Med. J.*, Vol. 22, No. 3, 210–215, 2016.

3. Köşüş, N., A. Köşüş, M. Duran, S. Simavlı, and N. Turhan, "Comparison of standard mammography with digital mammography and digital infrared thermal imaging for breast cancer screening," *Journal of the Turkish German Gynecological Association*, Vol. 11, No. 3, 152, 2010.

4. Heywang-Köbrunner, S. H., A. Hacker, and S. Sedlacek, "Advantages and disadvantages of mammography screening," *Breast Care*, Vol. 6, No. 3, 199–207, 2011.

5. Fernández, M. G., Y. Á. López, A. A. Arboleya, B. G. Valdés, Y. R. Vaqueiro, F. L. H. Andrés, and A. P. García, "Synthetic aperture radar imaging system for landmine detection using a ground penetrating radar on board a unmanned aerial vehicle," *IEEE Access*, Vol. 6, 45100–45112, 2018.

6. Selvaraj, V. and P. Srinivasan, "Interaction of an EM wave with the breast tissue in a microwave imaging technique using an ultra-wideband antenna," *Biomedical Research*, Vol. 28, No. 3, 1025–1030, 2017.

7. Kuwahara, Y. and A. M. Malik, "Microwave imaging for early breast cancer detection," *New Perspect. Breast Imaging*, 45–71, IntechOpen, 2017.

8. Zhang, H., S. Y. Tan, and H. S. Tan, "A novel method for microwave breast cancer detection," *2008 Asia-Pacific Microwave Conference*, 1–4, IEEE, 2008.

9. Chen, Y., E. Gunawan, Y. Kim, K. Low, and C. Soh, "UWB microwave imaging for breast cancer detection: Tumor/clutter identification using a time of arrival data fusion method," *2006 IEEE Antennas and Propagation Society International Symposium*, 255–258, IEEE, 2006.

10. Chen, Y., E. Gunawan, K. S. Low, S. C. Wang, C. B. Soh, and L. L. Thi, "Time of arrival data fusion method for two-dimensional ultrawideband breast cancer detection," *IEEE Transactions on Antennas and Propagation*, Vol. 55, No. 10, 2852–2865, 2007.

11. Ünal, İ, B. Türetken, and Y. Çotur, "Microwave imaging of breast cancer tumor inside voxel-based breast phantom using conformal antennas," *2014 XXXIth URSI General Assembly and Scientific Symposium (URSI GASS)*, 1–4, IEEE, 2014.

12. "Computer Simulation Technology (CST) microwave studio software," version 2010.

13. Tiang, S. S., M. S. Hathal, T. F. Zanoon, M. F. Ain, and M. Z. Abdullah, "Radar sensing featuring biconical antenna and enhanced delay and sum algorithm for early stage breast cancer detection," *Progress In Electromagnetics Research B*, Vol. 46, 299–316, 2013.

14. Borja, B., J. A. Tirado-Mendez, and H. Jardon-Aguilar, "An overview of UWB antennas for microwave imaging systems for cancer detection purposes," *Progress In Electromagnetics Research B*, Vol. 80, 173–198, 2018.

15. Amdaouch, I., O. Aghzout, A. Naghar, A. V. Alejos, and F. J. Falcone, "Breast tumor detection system based on a compact UWB antenna design," *Progress In Electromagnetics Research M*, Vol. 64, 123–133, 2018.

16. Adnan, S., R. Abd-Alhameed, C. H. See, H. I. Hraga, I. T. Elfergani, and D. Zhou, "A compact UWB antenna design for breast cancer detection," *PIERS Online*, Vol. 6, No. 2, 129–132, 2010.

17. AlShehri, S. A., S. Khatun, A. B. Jantan, R. S. A. Raja Abdullah, R. Mahmud, and Z. Awang, "Experimental breast tumor detection using NN-based UWB imaging," *Progress In Electromagnetics Research*, Vol. 111, 447–465, 2011.